Performance Evaluation on Map-based NDT Scan Matching Localization using Simulated Occlusion Datasets

Yin-Chiu, KAN.[1,2], Li-Ta, HSU.[1]*, Edward CHUNG.[2]*

[1] Interdisciplinary Division of Aeronautical and Aviation Engineering, The Hong Kong Polytechnic University, Hong Kong

[2] Department of Electrical Engineering, The Hong Kong Polytechnic University, Hong Kong

* Member, IEEE

Abstract— This letter presents a performance evaluation on the conventional normal distribution transform (NDT) map-based scan matching under the presence of occlusion. The LiDAR map-based localization method enables centimeter level accuracy positioning; however, the state-of-the-art algorithms do not achieve the same performance when excessive unexpected objects, such as pedestrians or dynamic vehicles, occlude the field of view (FOV) of the LiDAR. Although the NDT scan matching is able to cope with slight geometrical change of environment, the presence of unexpected objects still induces matching error due to the discrepancy created between the real-time scan and the pre-build map. In this study, we manually place bounding boxes into realistic medium-urban LiDAR scans to simulate occlusion scenarios and investigate the effect of the point cloud occlusion on the map-based NDT scan matching method performance. Under the occluded situations, the induced positioning error is found positively correlated to the change of heading angle. Significant 3D localization errors peaks, up to 42.41cm, are identified repeatedly at circumstances while the LiDAR encounters a substantial change of yaw angle, and these errors peaks amplify as the occlusion rate increases.

Index Terms—NDT Scan Matching, Point Cloud Occlusion, LiDAR, Localization, Autonomous Driving

I. INTRODUCTION

In highly dynamic urban environments, accurate positioning in a global positioning system (GPS) denied area is important for autonomous vehicles for path planning and perception missions. With the availability of high definition (HD) map, researchers have proposed different map-based localization methods to provide accurate and robust localization. LiDAR map-based normal distribution transform (NDT) scan matching is one of the major algorithms that has been being extensively used on autonomous vehicles and robotic applications. For example, Akai et al. used an extended Kalman filter (EKF) to fuse the poses of the map-based NDT localization and dead reckoning to increase the robustness [1]. One major disadvantage of the map-based NDT scan matching is that it is not robust against significant geometric change of environments or occlusion by excessive unexpected or dynamic objects [3]. These weaknesses highly affect the performance of map-based NDT scan matching. Previous studies [5],[8] found that NDT is able to cope with certain level of the environmental change. However, the localization accuracy of NDT still degrades when there are discrepancies between the environment and map. Such discrepancy could be introduced by the unexpected object occlusion (i.e. LiDAR sensor being partially blocked by pedestrian or other vehicles), which is unavoidable in highly dynamic urbanized cities, like Hong Kong [4].

In general, most of the previous works related to NDT [1],[3] study the impact of point cloud occlusion in the context of NDT-based simultaneous localization and mapping (SLAM) applications rather than map-based NDT. Out of the limited studies on map-based NDT, Wen et al. enhanced the uncertainty estimation performance of map-based NDT by modelling the surrounding dynamic vehicles [7]. Similarly, Akai et al. combined the estimated map-based NDT matching uncertainty information with a road-marker matching method using a particle filtering algorithm to provide accurate positioning in areas where NDT scan matching fails [9]. However, these studies did not provide a concrete evaluation on the relationship between point cloud occlusion and the map-based NDT performance. Therefore, this letter proposes to evaluate the performance of the conventional map-based NDT scan matching under the presence of the point cloud occlusion.

In this letter, we aim to specifically evaluate the correlation between the point cloud occlusion rate and the performance of the map-based NDT. We generate synthetic occlusion datasets, perform the conventional NDT map matching with the prebuild map, and evaluate the performance under different occluded scenarios.

The contributions of this letter are as follows:

1. This letter proposes to investigate the relationship between the localization accuracy of the map-based NDT scan matching and the point cloud occlusion rate.
2. Accurate initialization of the heading angle is critical to the convergence performance of NDT [9]. This letter analyzes the relationship between the performance of NDT map matching and the change of heading angle under occluded scenarios.

Corresponding author: L.T. Hsu (lt.hsu@polyu.edu.hk).

The rest of this letter is composed as follows. In Section II, we present the conventional NDT scan matching method and the synthetic occlusion dataset generation process. In Section III, we present the experimental platform and the map-based NDT localization performance of each occluded dataset. In Section IV, we give our discussion and conclusion.

II. METHODOLOGY

A. 3D Normal Map-based Distribution Transform (NDT)

In this letter, we follow the 3D NDT method developed by Magnusson et al. [6]. Details can be found in [6]. For map matching, a 3D normal distribution (ND) map is built in advance from the 3D point cloud map, which is represented as a voxel map, for which each voxel i contains the mean ($\mathbf{q}_i^m$) and covariance matrix($\mathbf{\Sigma}_i$). The goal of the matching process is to find an optimal transformation, $\mathbf{p} = \begin{bmatrix} \mathbf{T_x} & \mathbf{T_y} & \mathbf{T_z} & \mathbf{R_x} & \mathbf{R_y} & \mathbf{R_z} \end{bmatrix}^T$, that maps the input scan to the pre-built ND map. In our case, the input scan from the Velodyne HDL-32E is filtered with a 2m voxel grid (VG) filter. Then, we use the filtered points $(\mathbf{x_1}, \mathbf{x_2}, \dots, \mathbf{x_M})$ to match with the pre-built ND map by the following NDT score function (eqn. 1).

$$S(\mathbf{x}) = \sum_{i-1}^{M} \exp\left(-\frac{(\mathbf{x}_i' - \mathbf{q}_i^m)^T \mathbf{\Sigma}^{-1}(\mathbf{x}_i' - \mathbf{q}_i^m)}{2}\right) \qquad (1)$$
$$\mathbf{x}_i' = \mathrm{T}(\mathbf{x}_i, \mathbf{p})$$

where $\mathrm{T}(\mathbf{x}_i, \mathbf{p})$ maps $\mathbf{x}_i$ from the LiDAR frame to $\mathbf{x}_i'$ from the ND map frame by the transformation parameter $\mathbf{p}$. By maximizing the NDT score using gauss-newton method, the estimated pose $\mathbf{p}$ is obtained once convergence is achieved.

B. Synthetic Point Cloud Occlusion Dataset Generation

We propose to generate synthetic occluded dataset by placing simulated bounding boxes into the raw LiDAR scan to simulate the LiDAR's field of view (FOV) being blocked by unexpected objects, such as dynamic buses. We firstly place bounding boxes into the raw LiDAR scan. Then, we employ the ray-box intersection algorithm (Algorithm 1) developed by Williams et al. [10] to detect the ray-box intersection and modify the occluded point cloud to the closest intersection if intersection exists. Fig. 1 shows the top view of a laser scan before and after occluded by two simulated bounding boxes.
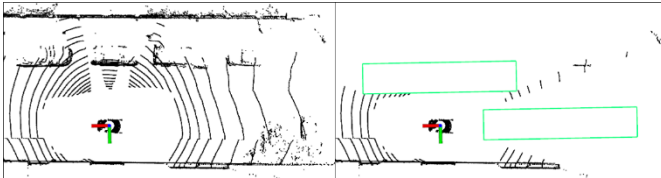

Fig. 1-Original LiDAR Scan (Left); Modified LiDAR Scan after two Simulated Bounding Boxes (Green) Being Placed (Right).

Below three steps show the synthetic occluded dataset generation process and the associated flowchart is shown in Fig. 2.
1. Applies NDT scan matching from the raw point cloud scan, then obtains and records the pose $\mathbf{p} = \begin{bmatrix} \mathbf{T_x} & \mathbf{T_y} & \mathbf{T_z} & \mathbf{R_x} & \mathbf{R_y} & \mathbf{R_z} \end{bmatrix}^T$ of LiDAR under map frame for each epoch.
2. Transforms the bounding box from map frame to LiDAR frame at each epoch using $\mathbf{p}$ from Step 1.
3. Performs point cloud modification using Algorithm 1 and outputs the modified dataset each epoch.

Algorithm 1

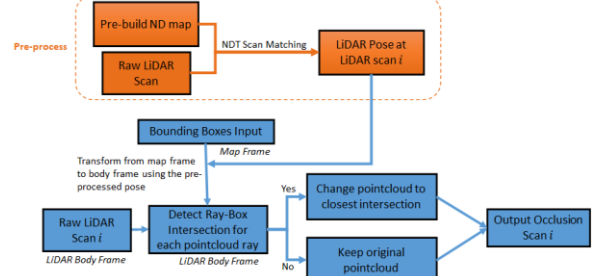|	
1	*Input: {raw LiDAR scan, Bounding Boxes (BB) Parameters}*
2	*Output: {modified LiDAR scan}*
3	For {each point cloud ray i in the original LiDAR scan}
4	if {point cloud ray i intersects any of the BBs' surfaces}
5	Find the ray-box closest intersection.
6	Modify the point cloud to the closest intersection.
7	end if
8	end

Fig. 2 – Flowchart for the synthetic occlusion dataset generation.

III. EXPERIMENTAL EVALUATION

To evaluate the effect of the point cloud occlusion on the map-based NDT scan matching, two synthetic scenarios generated from a realistic medium-urban dataset collected in Hong Kong are used.
1) High occluded (HO) case (mean occlusion rate $(\overline{\%occ}) > 60\%$)
2) Low occluded (LO) case ($\overline{\%occ} < 30\%$)

A. Experimental Setup

A Velodyne HDL-32E 32-channel 3D LiDAR sensor is used to provide the real-time point clouds at sampling frequency of 10Hz for the scan matching, and a NovAtel SPAN-CPT RTK/INS integrated navigation system is used to provide accurate position estimates for our experiment. To generate the point cloud map, we integrate the LiDAR odometry with the SPAN-CPT solution using the graph SLAM method by Koide et al [11]. In our case, real-time kinematic (RTK) fix was obtained by SPAN-CPT over the whole trajectory, so a high weighting factor was applied on SPAN-CPT in the information matrix to produce an accurate point cloud map as shown in Fig. 3.

The 3D positioning error (ϵ_{3D}) and the occlusion rate of point cloud ($\% occ$) are evaluated on both scenarios. Theoretically, the LiDAR scan matching shall perform better for non-occluded case than the occluded case, so the non-occluded case is treated as the baseline for comparison. The ϵ_{3D} between the occluded case and the baseline (non-occluded) case is computed by:

$$\epsilon_{3D} = \sqrt{(x_{occ} - x_{bl})^2 + (y_{occ} - y_{bl})^2 + (z_{occ} - z_{bl})^2} \qquad (2)$$

where subscripts *occ* and *bl* stand for the occluded case and baseline case, respectively. As map-based NDT scan matching process is to measure the similarity between the real-time point cloud and the pre-build point cloud map, the point cloud occlusion rate (% occ), computed by Eqn. (3), will be evaluated in Section IIIB.

$$\%occ = \frac{n_{occ}}{n_{total}} \times 100\% \qquad (3)$$

where n_{occ} and n_{total} denote the number of occluded point cloud and the total number of point cloud at each LiDAR scan, respectively.
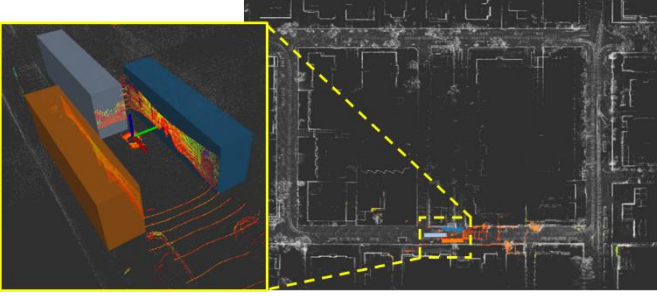
Fig. 3 – Demonstration of the point cloud map conducted in an urban area in Hong Kong and the bounding boxes placement for HO case.

B. Experimental Result

Table 1. Performance of NDT map-based scan matching at a high occluded (HO) case and low occluded (LO) case

		Longitudinal (cm)	Lateral (cm)	Altitude (cm)	2D (cm)	3D (cm)	Point. Cloud Occlusion (%)
HO	Mean	3.08	2.20	2.65	4.26	5.42	64.65
	Std	3.04	3.18	2.32	3.94	4.09	5.57
	Max	31.10	32.45	4.75	42.32	42.41	70.80
LO	Mean	0.89	0.77	0.63	1.31	1.55	29.44
	Std	1.22	1.35	0.84	1.72	1.84	3.05
	Max	10.69	14.23	11.87	15.44	15.67	33.44

High Occluded (HO) Case

In this experiment, three dynamic simulated bounding boxes are placed around the ego-vehicle at pre-defined offset distances. The size of each box is defined as 12.8m (L) x 2.5m (W) x 4.4m (H), which intends to simulate the standard double decker bus in Hong Kong. These three boxes move along with the ego-vehicle in the entire trajectory. Fig. 3 shows the bounding boxes distribution around the ego-vehicle. The total travelled distance of the whole experiment is more than 600m. The $\overline{\%occ}$ is 65.19%. A video demonstration of the HO case is available in the hyperlink in the footnote.[i]

In Fig. 4, the red curve shows the trajectory of the HO case in the top view, which generally matches well with the baseline case. As stipulated in Table 1, the mean ϵ_{3D} $\left(\overline{\epsilon_{3D}}\right)$ is only 5.42cm, and the associated standard deviation (std) is 4.09cm. Interestingly, the maximum ϵ_{3D} $\left(\epsilon_{3D,max}\right)$ is 42.41cm which is almost eight times higher than the mean error. It takes place at one of the corners in the trajectory as shown in the zoom in view of Fig. 4. To further evaluate the ϵ_{3D}, the top panel of Fig. 5 plots the ϵ_{3D} at each epoch. Four distinct error peaks could be identified, and they coincidently appears at the four corners of the trajectory. This possibly indicates that there is a relationship between the positioning error and the change of heading angle. The bottom panel of Fig. 5 plots the change of magnitude of the estimated yaw (heading) angle ($|\Delta\theta|$). It could be seen that the four peaks of the $|\Delta\theta|$ in the bottom panel well align with the four peaks of the ϵ_{3D} in the top panel. By computing the Pearson product-moment correlation coefficient ($r_{\epsilon_{3D},|\Delta\theta|}$) between the time series signal of the ϵ_{3D} and the $|\Delta\theta|$ using Eqn. (4), a correlation coefficient ($r_{\epsilon_{3D},|\Delta\theta|}$) of 0.6636 is obtained which indicates a moderate positive linear relationship between two signals.

$$r_{x,y} = \frac{\sum_1^n(x_i-\bar{x})(y_i-\bar{y})}{\sqrt{\sum_1^n(x_i-\bar{x})^2}\sqrt{\sum_1^n(y_i-\bar{y})^2}} \tag{4}$$

where *n* denotes sample size. x and y denote two individual signals. x_i and y_i denote individual samples and $\bar{x}$ and $\bar{y}$ denote the mean.

The middle panel of Fig. 5 plots the %occ at each epoch. No significant relationship between the ϵ_{3D} and %occ could be observed in Fig. 5.

By correlating the %occ with the ϵ_{3D}, a correlation coefficient ($r_{\epsilon_{3D},\%occ}$) of only 0.201 is obtained which confirms a weak linear relationship between the two signals. Interestingly, ϵ_{3D} is higher than the mean value at some places where %occ is lower than the average value, which contradicts the intuitive thinking. It is suspected that it is due to important map features were being occluded which significant degrades the localization accuracy. Such map features will be saved for valid map feature investigation in the future work.
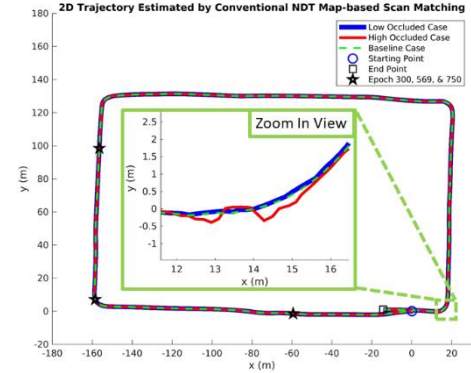

Fig. 4 - Estimated 2D Trajectory by NDT Map-based Scan Matching Method. Low Occluded Case (Blue Solid Line); High Occluded Case (Red Solid Line); Baseline Case (Green Dotted Line).
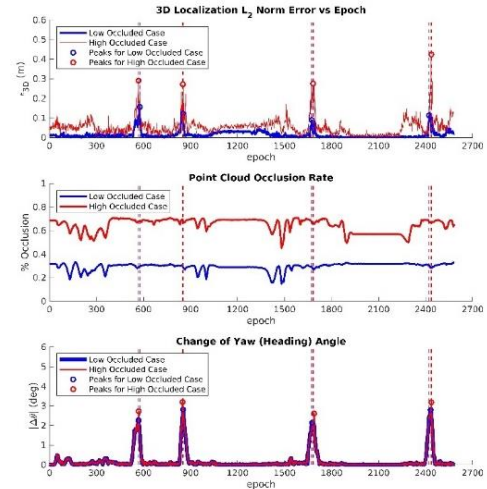

Figure 5 - ϵ_{3D} at each epoch (top); %occ at each epoch (middle); $|\Delta\theta|$ (bottom); Vertical line indicates the peaks alignment of ϵ_{3D} with $|\Delta\theta|$.

Low Occluded (LO) Case

Similar to the HO case, one dynamic box, with a size of 12.8m (L) x 2.5m (W) x 4.4m (H), is placed on the right side of ego-vehicle at a pre-defined offset distance for the LO case. The $\overline{\%occ}$ is 29.85%. A video demonstration of the LO case is available in the hyperlink in the footnote.[i] The $\overline{\epsilon_{3D}}$ is only 1.55cm, and the associated std is 1.84cm. Table 1 tabulates the individual localization errors and the %occ for this case.

Similarly, four distinct peaks of the ϵ_{3D} could be identified at the four corners, and they again well aligns with the peaks of the $|\Delta\theta|$ as

shown in Fig. 5, but the maximum $\in_{3D}$ reduces to 15.67cm from 42.42cm when compared to the HO case. A correlation coefficient $(r_{\epsilon_{3D},|\Delta\theta|})$ of 0.7176 is obtained which shows a moderate positive linear relationship between the $\in_{3D}$ and the $|\Delta\theta|$, whereas $r_{\epsilon_{3D},\%occ}$ of only -0.0835 is obtained. The nearly zero correlation coefficient indicates no linear relationship between two signals. This agrees with the observation in the HO case. To summarize, Table 2 tabulates the correlation coefficients that relate the $|\Delta\theta|$ and the $\%occ$ to the $\in_{3D}$.

Table 2. Correlation coefficients relate the magnitude of the yaw angle change and occlusion rate with 3D positioning error

	High Occluded Case	Low Occluded Case
$r_{\epsilon_{3D},|\Delta\theta|}$	0.6636	0.7176
$r_{\epsilon_{3D},\%occ}$	0.1902	-0.0835

To investigate the trivial results at sharp turns in Fig. 5, $\overline{\in_{3D}}$ and $\in_{3D,max}$ are further evaluated at the sharp turn occurring around epoch 569 with 31 different randomly generated occluded scenarios. NDT map matching is applied on the dataset from epoch 300 to epoch 750 for 31 different cases. The associated locations at epoch 300, 569, and 750 are marked in Fig. 4. In Fig. 6, $\overline{\in_{3D}}$ increases with $\overline{\%occ}$. For $\in_{3D,max}$, it shows that the error is generally small (i.e. $< 10cm$) for the $\overline{\%occ}$ less than 25%. In this region, no vivid error peaks could be identified during sharp turn. For $\overline{\%occ}$ between 25% and 80%, the errors rise as $\overline{\%occ}$ increases, and distinct error peaks could be observed at turns similar to the LO and HO cases. NDT matching was also applied on two cases with the $\overline{\%occ}$ exceeds 80%, no solutions were obtained due to divergence.

In Fig. 6, it is interesting to note that a 20cm difference of the $\in_{3D,max}$ occurs at $\overline{\%occ}$ around 75% even though the $\overline{\%occ}$ is approximately the same. It is suspected that is caused by the occlusion of important map features, for which we will leave it for further investigation in future works.
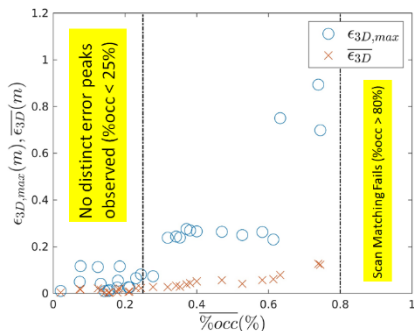

Fig. 6 – $\in_{3D,max}$ and $\overline{\in_{3D}}$ for 31 randomly generated occluded scenarios.

IV. DISCUSSION AND CONCLUSION

With the performance evaluation on the conventional NDT map matching method under occlusion, it is found as follows:

- Higher rate of occlusion would result a higher map-based NDT scan matching error generally. Increase of the mean 3D positioning error occurs as $\%occ$ rises of as shown in Fig. 6.
- The NDT localization error amplifies at sharp turns locally in our synthetic datasets. With the mean $\%occ$ higher than 25%, distinct positioning error peaks can be identified repeatedly when the LiDAR sensor undergoes substantial change of heading angle. A

moderate positive linear relationship between the $|\Delta\theta|$ and the $\in_{3D}$ is identified in both the HO and LO synthetic datasets.

It is commonly known that the performance of the NDT map matching degrades under occlusion. In this letter, it is particularly interesting that significant localization error amplifies locally when the LiDAR sensor is under substantial change of yaw angle. In the previous study by Akai et al. [9], the NDT convergence performance could easily fall into local minimum for inaccurate yaw angle initialization. With the additional uncertainty possibly introduces to the yaw angle estimated solution by the occlusion, it is suspected that the distinct error peaks are caused by the combined effects of the substantial change of yaw angle and the point cloud occlusion.

In summary, point cloud occlusion has a negative impact to the map-based NDT localization method. The evaluated results of this study can be a good starting point for further mitigating the effects of occlusion. For the future works, we will make use of the existing trivial results and further investigate the occlusion results in terms of valid map features [12] and scan shapes [13]. By relating the occlusion with the map features, we hope to better estimate the uncertainty for LiDAR-based localization method for a better sensor fusion estimated solution in the future.

REFERENCES

[1] W. Wen et al. Performance analysis of ndt-based graph slam for autonomous vehicle in diverse typical driving scenarios of Hong Kong. Sensors, 18(11):3928, 2018.

[2] N. Akai et al., "Autonomous driving based on accurate localization using multilayer LiDAR and dead reckoning," in Proceedings of the IEEE International Conference on Intelligent Transportation Systems (ITSC), pp. 1147–1152, 2017.

[3] Kanhere, Ashwin Vivek, Gao, Grace Xingxin, "LiDAR SLAM Utilizing Normal Distribution Transform and Measurement Consensus," Proceedings of the 32nd International Technical Meeting of the Satellite Division of The Institute of Navigation (ION GNSS+ 2019), Miami, Florida, September 2019, pp. 2228-2240.

[4] Wen, W.; Hsu, L.-T.*; Zhang, G. (2018) Performance analysis of NDT-based graph slam for autonomous vehicle in diverse typical driving scenarios of Hong Kong. Sensors 18:3928.

[5] P. Biber et al., "The normal distributions transform: A new approach to laser scan matching," IEEE/RSJ International Conference on Intelligent Robots and Systems, vol. 3, 2003.

[6] M. Magnusson et al., "Scan registration for autonomous mining vehicles using 3D-NDT," Journal of Field Robotics, vol. 24, no. 10, pp. 803-827, 2007.

[7] Wen, W., Bai, X., Zhan, W., Tomizuka, M., Hsu, L.T. (2019) Uncertainty Estimation of LiDAR Matching Aided by Dynamic Vehicle Detection and High Definition Map, IET Electronics Letters 55(6):348-349.

[8] M. Magnusson et al., "Evaluation of 3D registration reliability and speed - A comparison of ICP and NDT," IEEE International Conference on Robotics and Automation, 2009.

[9] N. Akai, L. Y. Morales, E. Takeuchi, Y. Yoshihara, and Y. Ninomiya, "Robust localization using 3D NDT scan matching with experimentally determined uncertainty and road marker matching," IEEE Intelligent Vehicles Symposium, 2017.

[10] A. Williams, S. Barrus, R. Keith, M. P. Shirley, "An efficient and robust ray-box intersection algorithm," Journal of Graphics Tools 10, 1 (2005), 49– 54.

[11] K. Koide, J. Miura and E. Menegatti, "A portable three-dimensional lidar-based system for long-term and wide-area people behavior measurement", International Journal of Advanced Robotic Systems, vol. 16, no. 2, pp. 1729881419841532, 2019.

[12] E. Javanmardi, M. Javanmardi, Y. Gu and S. Kamijo, "Pre-Estimating Self-Localization Error of NDT-Based Map-Matching From Map Only," in IEEE Transactions on Intelligent Transportation Systems, doi: 10.1109/TITS.2020.3006854.

[13] W. Zhen, S. Zeng and S. Soberer, "Robust localization and localizability estimation with a rotating laser scanner," 2017 IEEE International Conference on Robotics and Automation (ICRA), Singapore, 2017, pp. 6240-6245, doi: 10.1109/ICRA.2017.7989739.